Mechanics Research Communications 107 (2020) 103535

Contents lists available at ScienceDirect

Mechanics Research Communications

journal homepage: www.elsevier.com/locate/mechrescom

3D manufacturing of intracranial aneurysm biomodels for flow visualizations: Low cost fabrication processes

A. Souza[a,b,*], M.S. Souza[a,b], D. Pinho[c,d,h], R. Agujetas[e], C. Ferrera[e], R. Lima[d,f], H. Puga[c], J. Ribeiro[a,g]

[a] Instituto Politécnico de Bragança, Bragança, Portugal
[b] CEFET/RJ, Campus de Angra dos Reis, Rio de Janeiro, Brazil
[c] CMEMS, Minho University, Guimarães, Portugal
[d] MEtRICs, Mechanical Engineering Department, Campus de Azurém, University of Minho, Guimarães, Portugal
[e] Depto. de Ingeniería Mecánica, Energética y de los Materiales and Instituto de Computación Científica Avanzada, Universidad de Extremadura, Badajoz, Spain
[f] CEFT, FEUP, R. Dr. Roberto Frias, 4200-465 Porto, Portugal
[g] CIMO, Instituto Politécnico de Bragança, Bragança, Portugal
[h] INL—Inthernational Iberian Nanotechnology Laboratory, Av. Mestre JoséVeiga, 4715-330 Braga, Portugal

ARTICLE INFO

Article history:
Received 27 March 2020
Revised 10 May 2020
Accepted 11 May 2020
Available online 2 June 2020

Keywords:
Intracranial aneurysm
Biomodels
Manufacturing
Experimental mechanics
Computational fluid dynamics

ABSTRACT

There is a continuous search for better and more complete in vitro models with mechanical properties closer to in vivo conditions. In this work a manufacturing process, based on a lost core casting technique, is herein reported to produce aneurysm biomodels to perform experimental hemodynamic studies. By using real artery images combined with a lost core casting technique, three materials were tested: paraffin, beeswax and glycerin-based soap. All in vitro biomodels were compared according to their transparency and final structure. Additionally, comparisons between experimental and numerical flow studies were also performed. The results have shown that the biomodels produced with beeswax and glycerine-based soap were the most suitable in vitro models to perform direct flow visualizations of particulate blood analogue fluids. The biomodels proposed in this works, have the potential to provide further insights into the complex blood flow phenomena happening at different kinds of pathologies and answer to important hemodynamics questions that otherwise cannot be tackled with the existing in vitro models.

1. Introduction

Intracranial aneurysm (IA) is an abnormal dilation of a cerebral blood vessel resulting usually in a saccular form [1]. Its rupture affects 2.6% of the population and, it is the cause of 85% of subarachnoid hemorrhage [2]. Although the scientific community commonly agrees that the leading cause of IA onset is the weakening of the brain wall [2], the biological, physiological and biomechanical characteristics behind this weakening are still unknown [3]. Congenital disabilities such as aging, atherosclerotic changes, trauma, and infectious emboli may be the likely causes of this weakening [4]. Other factors related to the onset of the aneurysm are hypertension, smoking, and abuse of alcohol [5]. Moreover, internal blood flow pressure can also have an essential effect on aneurysm rupture [6]. Kristian Valen-Sendstad et al. [7], using an IA, have demonstrated by direct numerical simulation that turbulence in blood flow increases the wall shear stresses to their maximum values.

The study of aneurysm local hemodynamics is crucial to understanding their growth and complications. It will help in the postoperative period and the development of new treatment techniques [8]. As stated by previous research reports, introducing a stent it may distort local hemodynamics, and their impact should be understood [9]. For this reason, it is common to use different experimental approaches such as *in silico, in vivo* and *in vitro*. Numerical studies always require experimental validation. On the other hand, *in vivo* testing is very efficient, but it is enormously costly and involves ethical and reproducibility issues [10]. Finally, the use of *in vitro* experimental techniques may overcome the issues set by the previous approaches. Manufacturing biomodels, which reproduce with high accuracy the arterial geometries will allow experimental studies of fluid dynamics. This is mandatory to improve the clinical understanding of aneurysm growth, assisting in the preoperative treatment or improving the existing endovascular treatments.

* Correspondent author.
E-mail address: andrews.va.souza@alunos.ipb.pt (A. Souza).

https://doi.org/10.1016/j.mechrescom.2020.103535
0093-6413/

Biomodeling is the ability to transform biological models into real solid models using rapid prototyping (RP). This technology has been applied in IA since 1999, D'Urso et al. [11] constructed ABS solid biomodels of intracranial aneurysms to prove its viability to help in surgical planning. With the passage of time, this technique has been optimized, applying different materials and 3D printing techniques [12,13]. The biomodels have become flexible, hollow and anatomically closer to reality [14,15]. Nowadays, they are effective in assisting surgery, by reducing surgical time and the risk of death [16]. Nevertheless, they face serious limitations for the case of hemodynamic studies. As visualizing the inner flow is imperative, they must be transparent to white light, its thickness should be less than the focal length of the objective used for experimental testing [17] and the used material must have a refractive index as closest as possible to the fluid one [18].

Many researchers have developed *in vitro* techniques to enable experimental studies of blood flow in realistic configurations using direct rapid prototyping [19,20] or in the manufacture of negative molds [17,21]. However, it is difficult to choice the lost core (sacrificial) pattern material or to remove it, if one manufactures blood vessel biomodels uses negative molds [18]. The coating properties can be changed in high melting point materials. Some of them leave debris on the channel wall (cerrolow [22]) or have restrictions on small diameters (wax [23]). Although wax and cerrolow are the most widely used materials, there are several studies with other different materials such as isomalt [23], gelatin [18], and melted sucrose [17].

In this paper, is described the manufacturing process to create and replicate biomodels of an intracranial aneurysm in a millimeter-scale range. The models were produced from the lost core casting process using paraffin, beeswax and glycerin-based soap and were coated with an optically transparent polydimethylsiloxane (PDMS) material [6]. In addition, the quality of the manufactured PDMS biomodels was evaluated dimensionally, optically and through experimental comparison with numerical results obtained from CFD (Computational Fluid Dynamics) simulations. The low cost lost core, beeswax and glycerin-based soap materials, had not yet been used for this type of application and are suitable: not interact with the PDMS coating, and not need to be melted at high temperatures. The biomodels obtained showed that they have good reproducibility and are ideal for testing the visualization of flow-tracing particles. Therefore, they are suitable for hemodynamic tests and numerical validation.

2. Materials and methods

As we have just mentioned our main objective is to manufacture an IA PDMS biomodel suitable for flow analysis. This biomodel is subjected to several restrictions:

Dimensions, the channels of the biomodel must reproduce the curves and surfaces of the real artery.

Optics, the manufacturing material must be transparent, and its refractive index should be similar to the fluid used in the experiments.

Lost core material, its geometry must match the stereolithography (STL) geometry and it must be easily removable to avoid the presence of residuals in the biomodel.

Reproducibility, the manufacturing process should allow to build biomodels without any dimensional discrepancies.

We have imposed a final restriction using low cost materials and employing affordable processes in order reduce expenses and be economically viable.

A summary of the manufacturing process it is as follows: A set of angiographic medical images were acquired in the Hospital, then images were segmented with the ScanIP software from the company Synopsys® and a digital model of the aneurysm in STL format was obtained. This STL file was sent for prototyping stereolithography and a resin model was built. A bipartite silicone mold was produced using this model. Finally, that mold was used as cavity for three lost core materials: paraffin, beeswax and glycerin-based soap, which were removed at the end of the process. PDMS silicone is introduced as a final coating, giving rise to the transparent biomodel.

Table 1
Rapid prototyping specifications for the stereolithography process.

ProJet 1200	
Net build volume (xyz)	43 × 27 × 150 mm
Native Resolution (xy)	56 micron
Layer Thickness	0.03 mm
Vertical build speed up to	14 mm/hour
Post-processing	Bult-in UV curing station

The whole process allowed us to construct IA biomodels on the real scale. We also manufactured them in a 30% reduced scale. This step is necessary as we needed to test if the lost core materials were viable to manufacture smaller diameter channels and to allow different visualization tests in optical microscopes. In the following sections is described, in detail, the mentioned stages of the manufacturing process for IA PDMS biomodels.

2.1. Obtaining the digital model

Typical procedures to get non-invasive anatomical information for aneurysm are angiography, computed tomography or magnetic resonance. In this work, the anatomical area where the aneurysm is located was acquired by an angiography. The obtained images in the DICOM (Digital Imaging and Communications in Medicine) format were imported to software ScanIP. The thresholding technique was employed to identify the different structures of interest. These structures were labeled with four colors. Fig. 1a shows the aneurysm and several arteries. The right internal carotid artery (ICA)-R, its branches and the aneurysm were isolated from other structures (Fig. 1b). Then it was cut along with the anterior cerebral artery (ACA) and middle cerebral artery (MCA), (Fig. 1c). Finally, the obtained model was transformed into STL format (Fig. 1d).

2.2. Rapid prototyping of the 3D aneurysm mold

3D printing is capable of use different materials to produce molds, such as ABS, PLA, PVA, plaster powder, among others. However, latter changes in the mold geometry and its subsequent influence in the dimensions must be avoided. VisiJet FTX was chosen to prevent additional surface treatment with sandpaper, acetone, glue or varnishes. This material has a good surface finish, strength and can also be used directly as a sacrificial core [19].

Once the printing material was chosen, STL files were transferred to the 3D printer (ProJet 1200) and the master mold was printed by stereolithography. In this process, the printer uses a liquid photopolymer resin, which can be epoxy or acrylic and it is polymerized with the action of ultraviolet light or laser. The specifications of the 3D printer used are given in Table 1.

The master molds obtained, with real dimensions and 30% scale reduction, were used to construct the bipartite silicone mold that will be used to model the lost core materials of paraffin, beeswax and glycerine-based soap (Fig. 2).

2.3. Lost core casting process and PDMS biomodels

Paraffin lost core: in the process of lost wax casting, the paraffin is heated to 65° C and injected in its liquid state into the bipartite

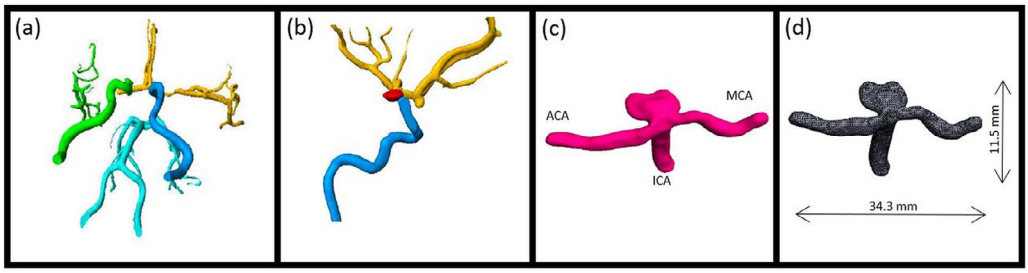

Fig. 1. Segmentation process of the arteries (a) Willys circle arteries; (b) aneurysm location; (c) vascular aneurysm anatomy obtained; (d) final aneurysm STL model.

Fig. 2. Rapid prototyping and lost wax. (a) rapid prototyping of VisiJet FTX Green resin (microsla); (b) bipartite silicone mold; (c) paraffin, glycerin-based soap and beeswax lost core pattern, respectively (full scale).

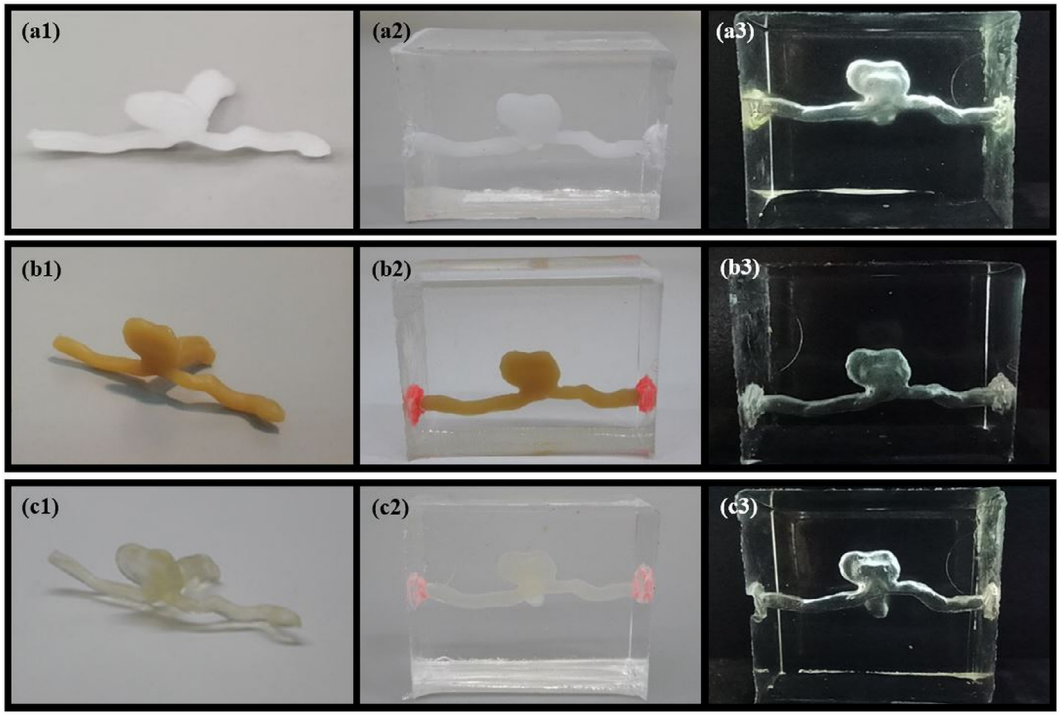

Fig. 3. Processing steps to obtain the final PDMS biomodel (a) paraffin; (b) beeswax; (c) glycerine-based soap.

silicone mold with a 3 mL syringe. After curing, the paraffin pattern is carefully removed from the bipartite mold (Fig. 3(a1)) and placed in an acrylic box, which is fixed to the wall using plasticine at its ends.

PDMS elastomer (Sylgard 184, Dow Corning) was the last material needed to manufacture the millimeter scale flow biomodels. This material has low refractive index and it is optically transparent for white light [20]. Prior to pouring PDMS into the acrylic box, where the mold is already positioned, the elastomer required an additional process. The elastomer was mixed with its curing agent in a ratio of 10:1 in a container. The resulting mixture was placed under vacuum conditions for 40 minutes to degas it and to eliminate the nucleated air bubbles present in the silicon. The result stood 48 h for its curation at room temperature (approximately 22° C) (Fig. 3(a2)). Finally, the PDMS transparent mold was heated 20 min in the oven a 75°C to dissolve the paraffin. Fig. 3(a3) shows the final transparent and hollow biomodel.

Beeswax lost core: for the manufacture of the PDMS biomodels using beeswax as a lost core pattern, the following steps were carried out. Beeswax was melted at 68° C and injected at that tem-

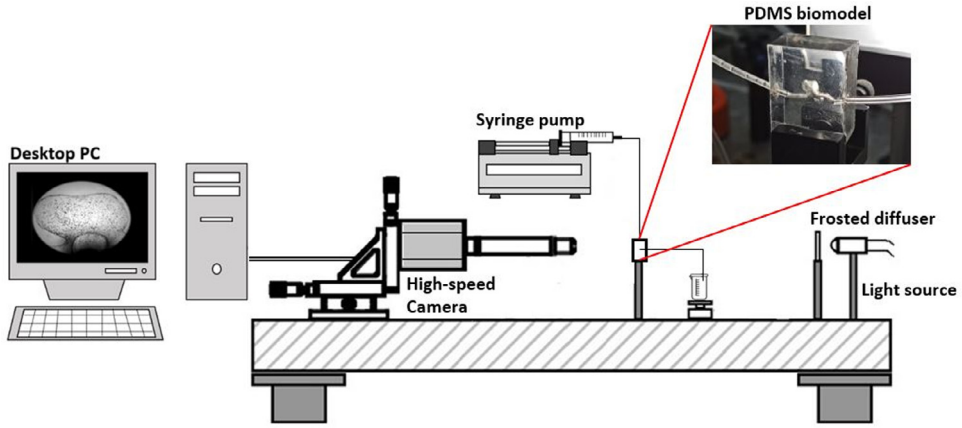

Fig. 4. Experimental setup to perform the flow experiments with the developed PDMS biomodels.

perature into the bipartite mold. After approximately 15 minutes, the pattern solidified and was removed from the split mold (Fig. 3 (b1)). Then, the same procedure as in the paraffin pattern was followed to create the PDMS mold (Fig. 3 (b2)). The beeswax pattern was removed mechanically (Fig. 3 (b3)).

Glycerin-based soap lost core: the third lost core pattern is shown in Fig 3 (c1). Glycerin-based soap was melted in an electric stove at 60°C and injected into the bipartite mold where it remained for 30 minutes for solidification. The manufacturing and curing PDMS process was similar to the previous ones (Fig. 3 (c2)). After curing, the glycerine-based soap pattern was dissolved in water at room temperature on a magnetic stirrer. Finally, the channels were cleaned with a water jet (Fig. 3 (c3)).

2.4. Flow visualizations setup and numerical simulations

To perform flow visualizations, it was used a high-speed video apparatus consisting of an ultra-high-speed CMOS camera (Photron, FASTCAM SA5) equipped with a set of optical lenses of a 1 × magnification zoom-objective (OPTEM Basic Module) and a system of lenses (Optem Zoom 70 XL) with variable magnification from 0.75 × to 5.25 × . The biomodel was illuminated from the back side by cool white light (Storz, Xenon Nova 300) and a frosted diffuser was positioned between the light and the biomodel to guarantee a field uniform illumination. The experimental set-up was mounted on an anti-vibration table (Fig. 4).

Following the work of Pinho et al. [24] and Campo-Deaño [25] a particulate based fluid was developed and applied to perform the flow experiments. This working fluid is composed by glycerol and water at 61% and 39%, respectively (w/w) and with 0.1% of 60 μm (in diameter) suspended polymethylmethacrylate (PMMA) particles. This fluid will be characterized through density, refractive index and viscosity measurements. All experiments were performed at room temperature (T = 20 ± 2°C).

The recorded images were processed using the ImageJ software and the particles trajectories were obtained using the Z Project plugin.

On the other hand, the fluid trajectories were obtained numerically. Both continuity and Navier-Stokes equations were solved using the commercial software Fluent, Ansys 2017. Stationary and uncompressible regime and rigid walls were prescribed. The working fluid was considered as a Newtonian fluid (Table 4).

Concerning the boundary conditions, the flow rate was imposed in the inlet section (MCA) and outflow in the outlet (ACA).

Four different flow rates were imposed to compare the experimental and numerical flows. The flow rates employed were: 5 mL/min, 10 mL/min, 15 mL/min and 20 mL/min. Low flow rates were considered as the recirculation appears and this allowed us to check properly the particles trajectories.

Table 2
Dimensions (mm) and the average error of original PDMS biomodel obtained with the three different sacrificial material.

	STL	Beeswax	Glycerin	Paraffin
A	2.587	2.390	2.425	2.364
B	2.897	2.725	2.784	2.756
C	8.392	8.775	8.877	8.817
D	2.122	1.947	2.005	1.875
E	2.693	2.505	2.522	2.460
Average Error	6.67%	5.56%	7.76%	

Once both the fluid and boundary conditions are studied, the following steps are followed: 1) The geometry is imported into Ansys Workbench, 2) an 83633 cells mesh is generated and 3) a pressure-based solver is used to solve the numerical integration.

It is important to note that: a) the velocity-pressure coupling was performed using the SIMPLE scheme, b) the spatial discretization of the pressure equation was conducted with the second order approximation, while the momentum equations were discretized with the second order upwind scheme, c) a number of iterations were imposed, but the simulation solutions converged earlier. Moreover, the residuals were set small enough and the stability of the streamlines was monitored with the number of iterations.

Finally, we analysed the results in a model whose cell number was twice the original one while keeping the same spatial distribution. A 3.5% deviation was observed when running this mesh test.

3. Results

3.1. Comparison of geometric structure

The biomodels geometries must match the original STL model. Five different locations in this model were chosen to be compared with the biomodels (Fig. 5(a)). The air contained within the inner channels provides optimum contrast to measure the biomodels dimensions from images acquired with an inverted microscope (Fig. 5(b)).

Image J software allowed us to perform measurements at the different locations. The average value was then compared with the dimensions of the original STL model. Tables 2 and 3 show the values of the dimensions and average errors calculated for the original and reduced biomodels, respectively.

Analyzing the obtained values, shown in Table 2, it can be observed that the differences between the transparent biomodels and the respective STL format are approximately 0.21 mm for the re-

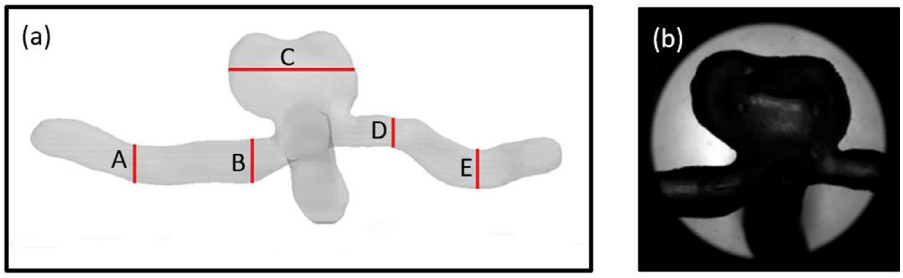

Fig 5. Schematic representation of the locations analysed: (a) in the STL model; (b) microscope image obtained to measure the location C.

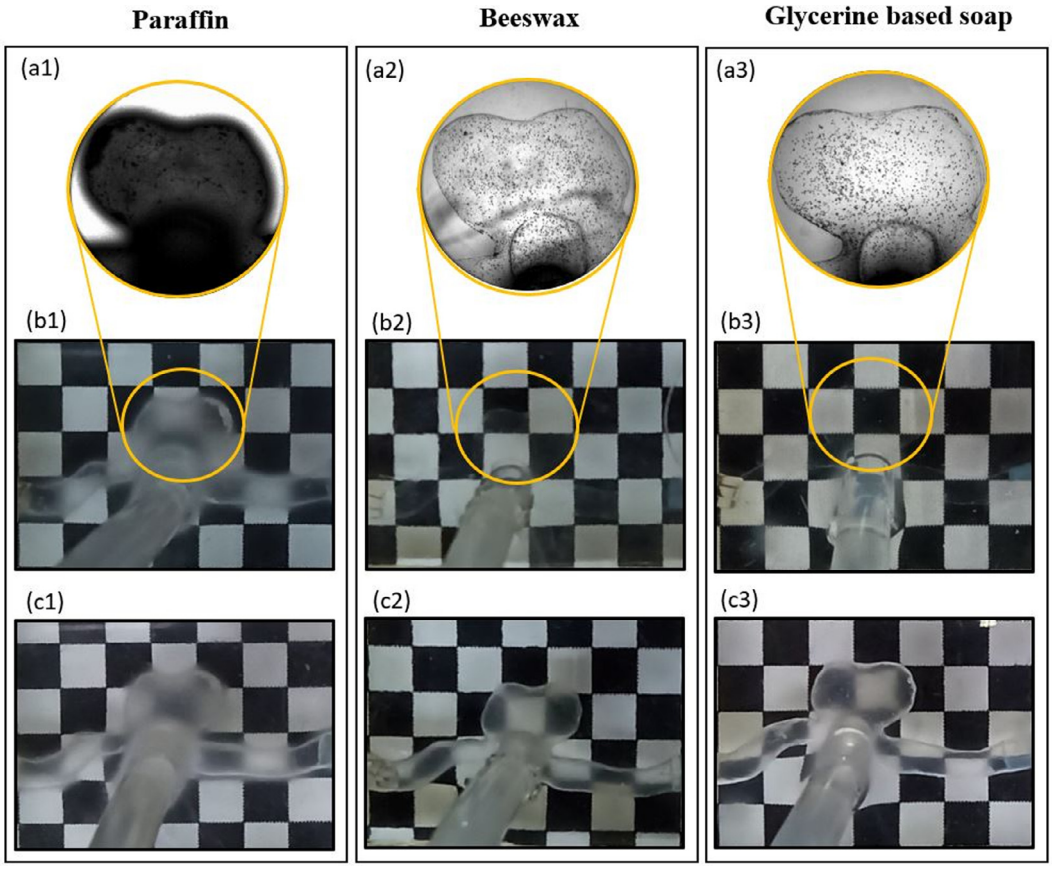

Fig. 6. Distortion of the grid lines. (a) detail of the particle visualization test; (b) distortion when the channel is filled with PMMA water/glycerol solution and (c) when it is filled with only water.

Table 3
Dimensions (mm) and the average error of reduced PDMS biomodel obtained with the three different sacrificial material

	STL	Beeswax	Glycerin	Paraffin
A	1.811	1.691	1.731	1.624
B	2.028	1.883	1.878	1.879
C	5.875	5.605	5.628	5.621
D	1.485	1.373	1.398	1.403
E	1.885	1.772	1.796	1.762
Average error	6.38%	5.33%	6.80%	

gions A, B, D and E and 0.42 mm for the region C, in the biomodel obtained by the lost core paraffin pattern. For the biomodel from the lost core beeswax, the differences were approximately 0.18 mm for A, B, D and E regions and 0.39 mm in C, and for the lost core glycerin-based soap biomodel, the difference was 0.14mm for A, B, D and E and 0.48mm for C.

The obtained values in the reduced biomodels, as show in Table 3, presented the differences in the channels of approximately 0.14 mm in A, B, D and E, and 0.25 in C in the case of the biomodel fabricated from the lost core paraffin pattern. For the biomodel manufacture from the lost core beeswax pattern, the differences were approximately 0.12 mm for A, B, D and E and 0.27 mm in C, and for the biomodel got with lost core glycerin-based soap pattern, the difference was 0.10 mm for A, B, D and E and 0.25 mm for C.

Furthermore, it can be observed that for both biomodels, original and the 30% reduced size, those that showed a smaller error in general, were the ones made with glycerin-based soap as a lost core material, followed by the biomodels beeswax, and finally those made with paraffin. It can also be observed that the reduced size biomodels presented a lower percentage of errors than the biomodels manufactured in real size, however this difference is very small, which allows saying that the manufacturing process

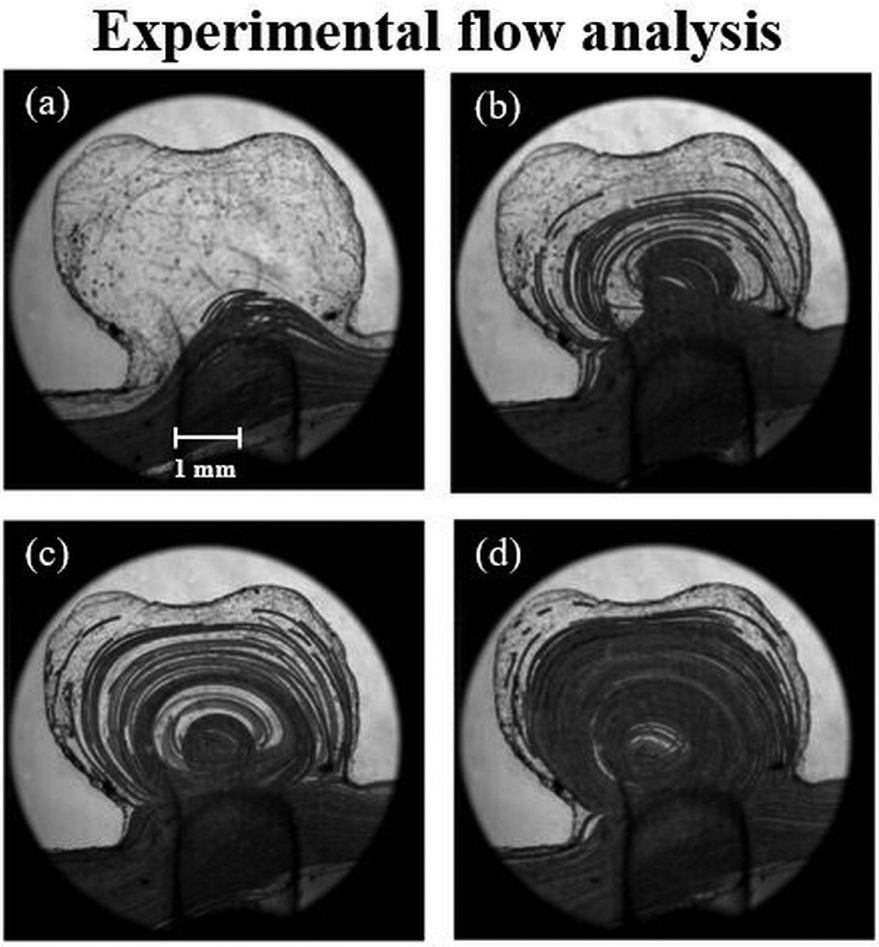

Fig. 7. Experimental flow analysis with flow rate of: (a) Q = 5 mL/min; (b) Q = 10 mL/min; (c) Q = 15 mL/min; (d) Q = 20 mL/min

Table 4
Physical properties of the materials used in this study.

Fluids	Refractive index	Viscosity (Pa.s)	Density (kg/m^3)
Water	1.333	0.920×10^{-3}	997
Water	1.412	1.290×10^{-2}	1153
PDMS	1.412	____	____

used permits to make reliable copies of the STL model and with good reproducibility.

3.2. Comparison of optical channel transparency

The second restriction is the need to perform flow visualizations in the developed PDMS biomodels. Both the refractive index of the PDMS and the fluid used in the experiments must be as close as possible. If the fluid refractive index is much lower than the PDMS, it appears a black distorted region next to the channel walls [25]. This distortion affects the particle visualization and it disappears completely when the refractive index of the fluid is similar to the PDMS. In this work, the refractive indices of PDMS and working fluids were measured using an Abbemat 500 refractometer. The fluid that matches the PDMS refractive index is composed by glycerol at 61% diluted (w / w) in water. The density of the mixture was measured with an Anton Paar 5000M densimeter and its viscosity a Cannon-Fenske viscometer. All the physical properties were measured at 25°C. Table 4 shows the values obtained by the solid-liquid interaction in the gridlines. The result of applying this technique, proposed by Hopkins et al. [26], is shown in Fig. 6. Two different tests were conducted. The first one checked if it was possible to see particles in the IA (Fig. 6a). It is quite difficult to see the particles when paraffin is employed in the manufacturing process (Fig. 6(a1)). To remove the paraffin in the PDMS biomodel, is necessary to melt it. The melted paraffin interacts with the PDMS and this process alters the biomodel optical properties. Nevertheless, the particles can be seen without problems when the mold is made of beeswax (Fig. 6(a2)) and glycerine based soap (Fig. 6(a3)). As it is not necessary to increase the temperature of the biomodel to withdraw these materials, the biomodel optics is not altered.

This is clearly seen in the second test. The fluid mixture is injected in the channels (Fig. 6b) and matches the PDMS biomodel refractive index except in the paraffin nuclei. The increase of temperature of the biomodel causes the refractive index alteration and the walls are clearly seen. In contrast, the biomodel disappear when the beeswax and glycerine are employed. If water is employed as fluid (Fig 6c), the fluid refractive index is lower than the PDMS one and the walls can be seen. Moreover, the straight gridlines (Figs. 6(b2) and 6(b3)) are distorted and a curvature appears (Fig. 6(c2) and (c3)).

4. Experimental and numerical fluid flow analysis

The previous section has shown that the biomodels manufactured using beeswax and glycerin-based soap are the ones suitable to perform optical hemodynamic studies.

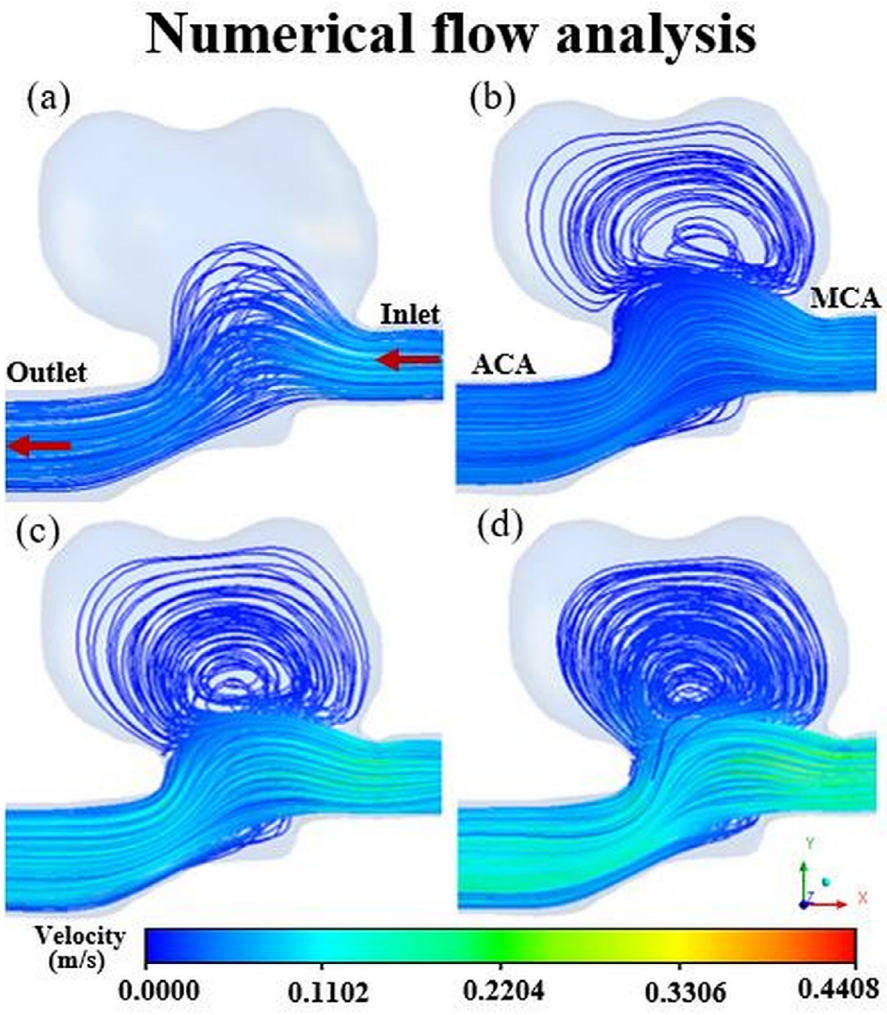

Fig. 8. Numerical flow analysis with flow rate of: (a) Q = 5 mL/min; (b) Q = 10 mL/min; (c) Q = 15 mL/min; (d) Q = 20 mL/min

Experiments and CFD analysis were also performed. The numerical simulation is a widely used tool to perform hemodynamic studies [27]. This tool has allowed us to perform qualitative comparisons of the streamlines obtained numerically with the experimental results.

4.1. Experimental procedure

As mentioned in Section 2.4, the reduced version of the PDMS biomodel was fixed, and a syringe pump with a 50 mL syringe was used to pump the working fluid at a constant flow rate within the channels of the biomodel. The PMMA trajectories resulting from the image process are shown in Fig. 7 (a)-(d).

4.2. Numerical simulation and qualitative comparison with the experimental

Once the particles trajectories were obtained, the STL format model dimensions were scaled down a 30% in Solidworks and exported to Parasolid format. This format was imported in the CFD analysis software and the numerical trajectories were obtained as it is described in Section 2.4.

In order to compare the results obtained in the experimental analysis with the numerical analysis, it was established as a criterion to observe the behaviour of the streamlines in both cases. The results obtained in both cases can be seen in Fig 7 and Fig 8. If a qualitative comparison is performed, the behavior of the fluid flow is nearly identical. A good agreement is shown in the regions close to the channel inlet and outlet where laminar flows were observed. Furthermore, the agreement remains when the flow behavior changed. If the trace particles get closer to the neck of the aneurysm, the flow bends towards the aneurysm and vortices are observed for the tested flow rates (except the lowest one (5mL/min)). This recirculation increases its intensity for the higher velocities. All these structures are pretty similar in both the experiments and numerical simulations.

5. Conclusions

To improve our understanding about the blood flow behavior in blood vessels, in vitro flow studies have a crucial role. Hence, the main objective of this study was to propose a manufacturing method from real flow biomodels, at the millimeter scale and suitable for hemodynamic studies. Generally, these kinds of biomodels were manufactured by means of a lost core casting method for their sacrificial material for each application.

The fabrication of the biomodels was made by using three lost core materials, paraffin, beeswax and glycerin-based soap that can be removed without high temperatures and can be modeled in silicone molds. The materials used as beeswax and glycerine-based soap, which were removed manually and in water at room temperature, respectively, reproduces biomodels with optimum optical

characteristics and no residues. However, the produced biomodels using paraffin have low optical transparency at room temperature. Overall, all the lost core materials have shown an adequate geometrical replication from the DICOM images and the average relative error of the main dimensions were less than 8%, being the smaller model with an error, less than 7%.

The developed PDMS biomodels were able to mimic the real artery geometry and could be easily replicated with high enough transparency to perform flow visualization studies. The flow measurements performed with the biomodel were in good agreement with CFD numerical simulations. Hence, this work shows that the proposed biomodels have the potential to be used as in vitro models to study complex hemodynamics phenomena happening in different kinds of pathologies such as aneurysms and stenotic blood vessels.

Acknowledgments

This work has been supported by FCT – Fundação para a Ciência e Tecnologia within the R&D Units Project Scope: UIDB/00319/2020, UIDB/04077/2020, UIDB/00690/2020 and NORTE-01-0145-FEDER-030171, funded by COMPETE2020, NORTE 2020, PORTUGAL 2020 and FEDER, R.A and C.F.acknowledge the support of Junta de Extremadura through Grants GR18175 and IB16119 (partially financed by FEDER) This project has received funding from the European Union's Horizon 2020 research and innovation programme under the Marie Sklodowska-Curie grant agreement No 798014. This project has received funding from the European Union's Horizon 2020 research and innovation programme under grant agreement No 828835.

Supplementary materials

Supplementary material associated with this article can be found, in the online version, at doi:10.1016/j.mechrescom.2020.103535.

References

[1] C. Rodriguez-Régent, et al., Non-invasive diagnosis of intracranial aneurysms, Diagn. Interv. Imag. 95 (12) (2014) 1163–1174, doi:10.1016/j.diii.2014.10.005.
[2] S. Sathyan, et al., Association of Versican (VCAN) gene polymorphisms rs251124 and rs2287926 (G428D), with intracranial aneurysm, Meta Gene 2 (2014) 651–660, doi:10.1016/j.mgene.2014.07.001.
[3] D. Pinho, D. Bento, J. Ribeiro, R. Lima, An in vitro experimental evaluation of the displacement field in an intracranial aneurysm model, Mech. Mach. Sci. 24 (June) (2015) 261–268, doi:10.1007/978-3-319-09411-3.
[4] F. Caranci, F. Briganti, L. Cirillo, M. Leonardi, M. Muto, Epidemiology and genetics of intracranial aneurysms, Eur. J. Radiol. 82 (10) (2013) 1598–1605, doi:10.1016/j.ejrad.2012.12.026.
[5] G. Tromp, S. Weinsheimer, A. Ronkainen, H. Kuivaniemi, Molecular basis and genetic predisposition to intracranial aneurysm, Ann. Med. 46 (8) (2014) 597–606, doi:10.3109/07853890.2014.949299.
[6] C. Cardoso, C.S. Fernandes, R. Lima, J. Ribeiro, Biomechanical analysis of PDMS channels using different hyperelastic numerical constitutive models, Mech. Res. Commun. 90 (2018) 26–33, doi:10.1016/j.mechrescom.2018.04.007.
[7] K. Valen-Sendstad, K.A. Mardal, M. Mortensen, B.A.P. Reif, H.P. Langtangen, Direct numerical simulation of transitional flow in a patient-specific intracranial aneurysm, J. Biomech. 44 (16) (2011) 2826–2832, doi:10.1016/j.jbiomech.2011.08.015.
[8] H. Baek, M.V. Jayaraman, P.D. Richardson, G.E. Karniadakis, Flow instability and wall shear stress variation in intracranial aneurysms, J. R. Soc. Interface 7 (47) (2010) 967–988, doi:10.1098/rsif.2009.0476.
[9] B.B. Lieber, A.P. Stancampiano, A.K. Wakhloo, Alteration of hemodynamics in aneurysm models by stenting: influence of stent porosity, Ann. Biomed. Eng. 25 (3) (1997) 460–469, doi:10.1007/BF02684187.
[10] W.M.P.F. Bosman, et al., Aortic customize: An in vivo feasibility study of a percutaneous technique for the repair of aortic aneurysms using injectable elastomer, Eur. J. Vasc. Endovasc. Surg. 40 (1) (2010) 65–70, doi:10.1016/j.ejvs.2010.02.019.
[11] P.S. D'Urso, et al., Cerebrovascular biomodelling: a technical note, Surg. Neurol. 52 (1999) 490–500, doi:10.1080/713842980.
[12] G. Wurm, B. Tomancok, P. Pogady, K. Holl, J. Trenkler, Cerebrovascular stereolithographic biomodeling for aneurysm surgery: Technical note, J. Neurosurg. 100 (1) (2004) 139–145, doi:10.3171/jns.2004.100.1.0139.
[13] A. Leal, M. Souza, P. Nohama, Additive manufacturing of 3D biomodels as adjuvant in intracranial aneurysm clipping, Artif. Organs 43 (1) (2019) E9–E15, doi:10.1111/aor.13303.
[14] Y. Kang, et al., Three-dimensional printing technology for treatment of intracranial aneurysm, Chin. Neurosurg. J. 2 (1) (2016) 1–10, doi:10.1186/s41016-016-0046-3.
[15] J.R. Ryan, K.K. Almefty, P. Nakaji, D.H. Frakes, Cerebral aneurysm clipping surgery simulation using patient-specific 3D printing and silicone casting, World Neurosurg. 88 (2016) 175–181, doi:10.1016/j.wneu.2015.12.102.
[16] B.O. Erbano, et al., Rapid prototyping of three-dimensional biomodels as an adjuvant in the surgical planning for intracranial aneurysms, Acta Cir. Bras. 28 (11) (2013) 756–761, doi:10.1590/S0102-86502013001100002.
[17] E. Doutel, J. Carneiro, M.S.N. Oliveira, J.B.L.M. Campos, J.M. Miranda, Fabrication of 3d mili-scale channels for hemodynamic studies, J. Mech. Med. Biol. 15 (1) (2015) 1–21, doi:10.1142/S0219519415500049.
[18] S.G. Yazdi, P.H. Geoghegan, P.D. Docherty, M. Jermy, A. Khanafer, A review of arterial phantom fabrication methods for flow measurement using PIV techniques, Ann. Biomed. Eng. 46 (11) (2018) 1697–1721, doi:10.1007/s10439-018-2085-8.
[19] A.V. Souza, J.E. Ribeiro, R. Lima, Manufacturing process of a brain aneurysm biomodel in PDMS using rapid prototyping, Lect. Notes Comput. Vis. Biomech. 34 (2019) 671–676, doi:10.1007/978-3-030-32040-9_69.
[20] P.H. Geoghegan, N.A. Buchmann, C.J.T. Spence, S. Moore, M. Jermy, Fabrication of rigid and flexible refractive-index-matched flow phantoms for flow visualisation and optical flow measurements, Exp. Fluids 52 (5) (2012) 1331–1347, doi:10.1007/s00348-011-1258-0.
[21] J.R. Sherman, et al., Investigation of new flow modifying endovascular image-guided interventional (EIGI) techniques in patient-specific aneurysm phantoms (PSAPs) using optical imaging, Med. Imag. 2008 Vis. Image-Guided Proc. Model. 6918 (69181) (2008) 69181, doi:10.1117/12.772583.
[22] R.F. Smith, B.K. Rutt, D.W. Holdsworth, Anthropomorphic carotid bifurcation phantom for MRI applications, J. Magn. Reson. Imaging 10 (4) (1999) 533–544, doi:10.1002/(SICI)1522-2586(199910)10:4⟨533::AID-JMRI6⟨3.0.CO;2-Z.
[23] L. Allard, G. Soulez, B. Chayer, F. Treyve, Z. Qin, G. Cloutier, Multimodality vascular imaging phantoms: a new material for the fabrication of realistic 3D vessel geometries, Med. Phys. 36 (8) (2009) 3758–3763, doi:10.1118/1.3171692.
[24] D. Pinho, L. Campo-Deaño, R. Lima, F.T. Pinho, In vitro particulate analogue fluids for experimental studies of rheological and hemorheological behavior of glucose-rich RBC suspensions, Biomicrofluidics 11 (5) (2017), doi:10.1063/1.4998190.
[25] L. Campo-Deaño, R.P.A. Dullens, D.G.A.L. Aarts, F.T. Pinho, M.S.N. Oliveira, Viscoelasticity of blood and viscoelastic blood analogues for use in polydymethylsiloxane in vitro models of the circulatory system, Biomicrofluidics 7 (3) (2013), doi:10.1063/1.4804649.
[26] L.M. Hopkins, J.T. Kelly, A.S. Wexler, A.K. Prasad, Particle image velocimetry measurements in complex geometries, Exp. Fluids 29 (1) (2000) 91–95, doi:10.1007/s003480050430.
[27] R. Agujetas, C. Ferrera, A.C. Marcos, J.P. Alejo, J.M. Montanero, Numerical and experimental analysis of the transitional flow across a real stenosis, Biomech. Model. Mechanobiol. 16 (4) (2017) 1447–1458, doi:10.1007/s10237-017-0898-2.